Torsional active-passive dampers on rotational machinery

Guillaume Paillot, Etienne Besnier, Simon Chesne, Didier Rémond

Torsional active-passive dampers on rotational machinery

Guillaume Paillot, Etienne Besnier, Simon Chesné, and Didier Rémond

Univ Lyon, INSA Lyon, CNRS, LaMCoS, UMR5259, 69621 Villeurbanne, France

Abstract

Recent hybrid control concepts, mixing active control with a fail-safe passive device, have drawn attractivity as they benefit from a theoretical hyperstability, ensuring very high stability margins. However, they have been experimentally tested until now only for the control of bending vibrations. The main purpose of this paper is to prove the performance of such systems also on torsional vibrations, with a specifically designed electromagnetic device, in order to contemplate the possibility to use them also for rotating machinery. As these control laws are model-free and require the adjustment of a few parameters related to the passive damper only, we demonstrate here their ease of integration for an application in rotating machines and we exhibit a direct experimental validation on an academic test bench. The latter which enables this experience despite the peculiarities of the rotation is therefore described, and the torsion reduction permitted by the hybrid control laws is assessed. A comparison between two of the newest hybrid control laws is also provided, proving the robustness and performance of these two hyperstable control laws. The main control parameters have been investigated and the performances are given through classical indicators but also in terms of energy consumption.

Keywords

Tuned Mass Damper; Torsion; Active vibration control; Hybridization; Rotating machinery

Introduction

The introduction of active control laws for vibration mitigation has largely improved the damping performance of such devices compared to conventional dampers. One of their other main advantages is their broadband action, especially when compared to Tuned Mass Dampers (TMD), that are efficient only on a narrow bandwidth around the critical frequency of the targeted mode. However, such active devices often face stability issues, and do not provide a damping capability in case of failure (Preumont et al., 2014).

To overcome the limited performance of TMDs, many authors have proposed to hybridize these dampers (Hybrid Mass Damper (HMD)) to an active system, most of the time using an electromagnetic transducer, such as a Voice Coil acting as the moving mass of the damper. The list of control strategies is therefore quite long: backstepping control (Umutlu et al., 2020), H_∞ robust control (Cao and Li, 2012), dual loop configuration (Chesné et al., 2019; Preumont and Seto, 2008), pole placement (Tso et al., 2013), fuzzy neural network algorithm (Yan et al., 2020), and so on. Hybridization of the control system has also been successfully developed for vibration isolation in helicopters (Rodriguez et al., 2018) using feedforward approaches. Applications for civil engineering (Preumont et Seto, 2018; Meinhardt et al., 2017) or for boat stabilization (Alujevic et al., 2020) have also been proposed. Recently, the resonant

device of hybridization has been off-set in the electrical domain to improve active control performance and reduce electrical requirements (Paknejad et al., 2021). The coupling between the electrical and mechanical domains to improve absorber performance has also been exploited to adjust absorber parameters (Cadioux et al., 2022), this coupling is of particular interest for tuning nonlinear absorbers. However, the stability of the hybrid systems needs to be carefully assessed (Collette and Chesné, 2016).

More related to torsion vibration control, many classical applications used TMD and a huge literature is dedicated to various architectures in the automotive industry. The hybridization of these passive solutions is on the way in two main directions, apart from electromagnetic actuators, with the use of MR fluids or non-linear dampers. For the first alternative, recent works confirm its interest for an automotive application (Dong et al., 2020; Gao et al., 2019; Wang et al., 2022). This technology can also be hybridized with centrifugal pendulums to further improve damping capabilities (Abouobaia et al., 2020). For the second alternative, one can refer the use of non-linear dampers, notably those testing both vibro-impact, cubic stiffness and higher order NES for automotive application (Haris et al., 2020). We can also mention the contribution of (Ahmadabadi, 2019) on the fixation of a NES to the crankshaft or of (Qiu et al, 2018) on a conical spring system.

For electromechanical solutions, (Auleley et al., 2021] investigates several architectures of shunts mounted on a TMD. More recently, (Dehaeze and Colette, 2021) presents modifications on the integral force feedback, considering inertial effects, to actively damp a rotating platform using piezoelectric stacks. The study of (Hosek et al., 1999) focuses on extending the action of centrifugal pendulums by forcing a delay by electromagnetic actuator, however potentially sensitive to stability problems. In addition (Aguirre et al., 2012) proposes a self-tuning ring damper, while (Lai et al., 2018) proposes the optimization of the behavior of tuned dampers by semi-actively driving their phase.

Hyperstable control laws, presenting infinite gain margin, are therefore very useful on such hybrid devices but it is not always easy to adapt them to the real systems. Recent research has proved two of them to be both efficient and easy to implement (pole placement α-HMD strategy (Chesné and Collette, 2018) and Skyhook damper emulation (Chesné, 2022)), even though the theoretical hyperstability has been lost during the experiment (despite very high remaining stability margins). However, experiments on these two control laws have been conducted only on bending vibrations. As the hybrid dampers are also relevant against torsional vibrations affecting rotating shafts, the purpose of this paper is to investigate the capabilities of the two aforementioned laws on a torsional test bench. It is also an experimental extension of a previous self-supplied hybrid damper (Paillot et al., 2023), seen as an original implementation of robust control laws in rotating machinery directly with experiments. The construction of the test rig is first described, then principle background on the laws is introduced. The evaluation is conducted under steady regime conditions: the speed oscillates around a constant target speed because of the torque fluctuations. The selected criterium for the performance evaluation is the magnitude of torsional vibrations at a given frequency. The two control strategies are then demonstrated to be efficient and robust with a few parameters to set-up. They are then compared to the passive TMD, both in terms of vibration mitigation and output current as consumption criteria of efficiency.

Description of the test rig

This test rig has been designed as a very first prototype and a proof-of-concept of an integrated solution including a permanent magnetic machine which is out of the scope of this paper. The development of the integrated machine and its characterization is described in a dedicated paper without any active control of the TMD (Paillot et al., 2023). Moreover, during the tests performed with this prototype, the authors were very careful and cautious not to exceed the resistance limits of parts which were manufactured in an additive manner with plastics (PLA). It is therefore very difficult to give some

insights about statistics and robustness of the proposed application of well-known control strategy to a rotating application.

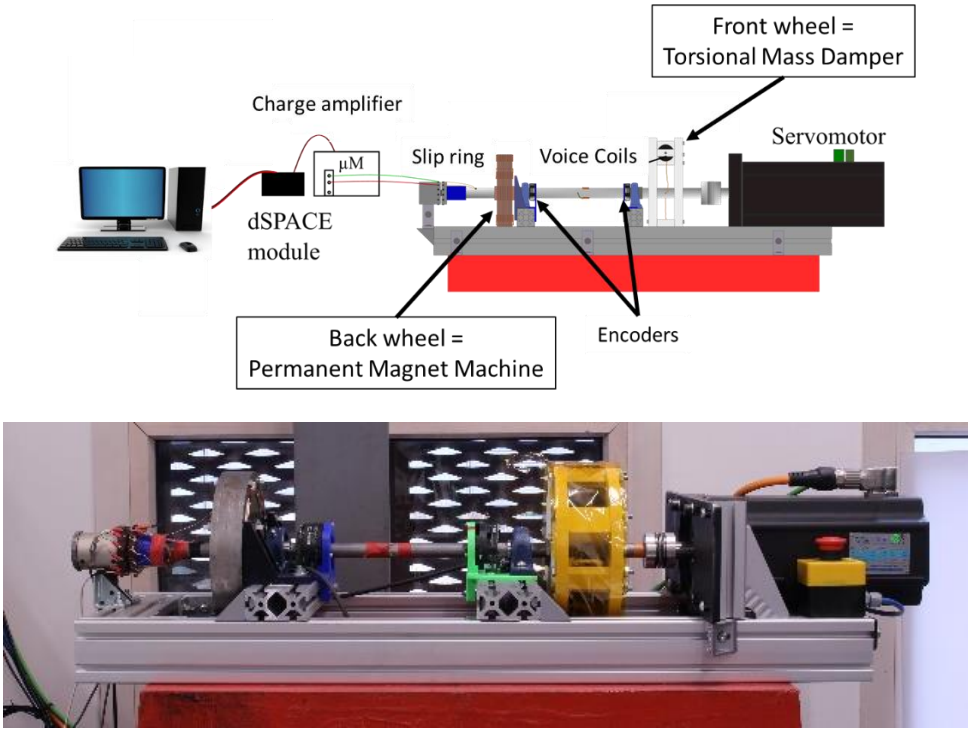

Figure 1. Sketch and picture of the test bench

All tests are run on a dedicated torsional test bench, depicted in Figure 1. It consists in two wheels linked together by a steel tube, a slipring, a servomotor (5.2 kW, nominal torque 20.6 N.m at 3000 rpm), two encoders, and a MicroMega ADD current amplifier.

The front wheel, made out of PLA (polylactic acid), embeds two electromagnetic Voice Coil actuators (MotiCont GVCM 051-032-01) squeezed between compression springs installed tangentially. The whole assembly is shown in Figure 2. They are electrically connected in series, and disposed symmetrically with respect to the axis of rotation to ensure the equilibrium of the part. Their contributions are cumulative, which is equivalent to the situation where only one device is installed. This wheel has a radius of 120 mm.

The second one is an assembly of steel plates, with a total thickness of 41mm and a radius of 90mm. As for the steel tube, a hollow shaft is indeed necessary for the electric circuit connecting the unembedded current amplifier to the actuators through the slipring. The steel tube radius is 20mm, with a wall thickness of 1.5mm. The total torsional length is 470mm. All inertia and stiffness values can be found in Table 1. Two encoders ((Heidenhein ERO 1324) offering a resolution of 2000 pulses per revolution are used for a precise angular position of two sections of the shaft. The encoder signals are directly processed in the DSpace system.

Part	Stiffness	Inertia
Front wheel	-	0.0184 kg.m²
Back wheel	-	0.0311 kg.m²
Torsion tube	1238.4 N.m	-
Voice Coils	81.83 N.m	0.0018 kg.m²

Table 1: Values of the different parameters

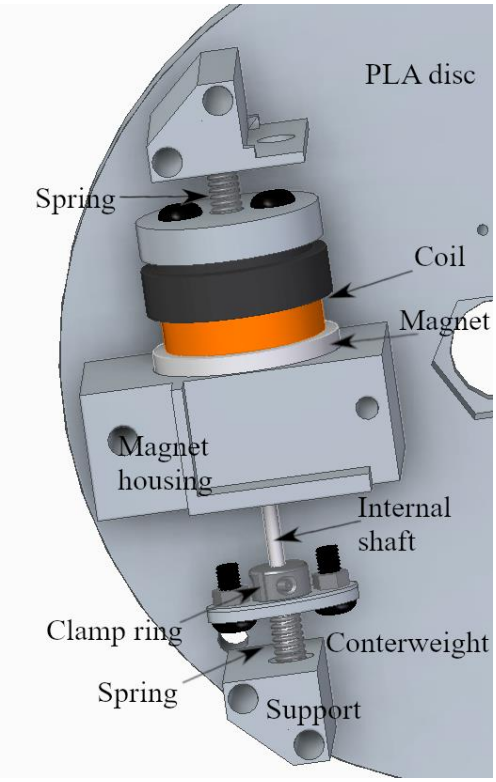

Figure 2. Assembly of the Voice Coil as a HMD on the test rig

With the values listed in Table 1, the frequency of the first torsional mode is $f_c = 52\,Hz$. The corresponding mode shape, in which the two wheels oscillate in opposition, shows that the larger displacement is to be found at the front wheel, which has the lower inertia, hence the location of the Voice Coils at the front. In this configuration, the equations of motion are:

$$\begin{cases} I_1\,\ddot{\theta}_1 + c_{eq}(\dot{\theta}_1 - \dot{\theta}_2) + k_{eq}(\theta_1 - \theta_2) + c_T(\dot{\theta}_1 - \dot{\theta}_{VC}) + k_T(\theta_1 - \theta_{VC}) + C_a = T_i \\ I_2\,\ddot{\theta}_2 + c_{eq}(\dot{\theta}_2 - \dot{\theta}_1) + k_{eq}(\theta_2 - \theta_1) = 0 \\ I_{VC}\,\ddot{\theta}_{VC} + c_{VC}(\dot{\theta}_{VC} - \dot{\theta}_1) + k_{VC}(\theta_{VC} - \theta_1) - T_a = 0 \end{cases} \quad (1)$$

In which the *VC* subscript refers to the Voice Coil. Figure 3 is a tentative illustration for the meaning of all parameters listed. The value of the actuator torque T_a depends on the control law, and T_i is the oscillating input torque that excites the system. Both are specified in the next section.

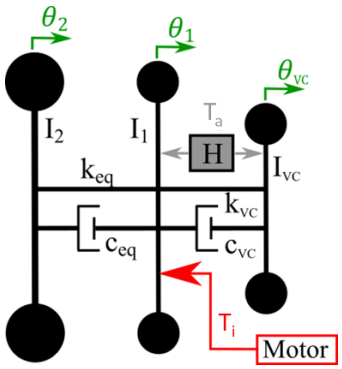

Figure 3. Simplified model of the demonstrator

The tuning of the TMD may differ due to the torsional condition. According to Den Hartog's theory (Ormondroyd and Den Hartog, 1928), we have:

$$\begin{cases} \mu = \frac{I_{VC}}{I_{eff}} \\ k_{VC} = I_{VC}.\left(\frac{2\pi.f_c}{1+\mu}\right)^2 \\ c_{VC} = 2.I_{VC}.\frac{2\pi.f_c}{1+\mu}.\sqrt{\frac{3\mu}{8(1+\mu)}} \end{cases} \quad (2)$$

Where μ represents the tuning parameter, which governs the shape of the modified transfer function and determines the inertia I_{VC}, and f_c is the frequency to be damped. However, these equations are approximations of the exact closed-form solutions, which have been established recently for torsional dampers by Nguyen and Vu, using several methods (Fixed point (Vu et al., 2017), Minimum Kinetic Energy (Nguyen, 2019), Minimum Quadratic Torque, Maximization of Equivalent Viscous Resistance and Fixed point (Nguyen, 2020)). The resulting optimal solutions are variable depending on the method adopted, especially when the inertia ratio increases, which makes them inconvenient to use, and the equations (2) are consequently preferred. In the experimental validation, these theoretical values are whatever not exactly respected, especially for the damping parameter: a characterization using the quality factor after a chirp excitation proved it to be about a third of its theoretical value. But for the stiffness parameter, the application of these methods may be used by analogy on a torsional damper in revolution.

Control and assessment

The rig is actuated by a three-phase PHASE Ultract servomotor, with a power of 5.2 kW. The torque C_i is exerted on the front wheel, and consists in a constant part, to provide a rotation at a given mean regime, and in an oscillating part, which magnitude, phase and frequency can be freely chosen. The rotation speed is measured by the motor encoder, and filtered out to access only the mean speed in the feedback loop. This prevents any interaction between the two parts, and enables a safe torsional shake at the required regime. The instantaneous angular speed at the two wheels is measured by Heidenhain ERO 1324-2000 encoders, and is also oscillating because of the non-stationary rotation conditions. These encoders are also able to measure the torsion along the shaft, by differentiation of the two corresponding angular positions. The precision of this measure is given by the relationship (3) (Remond, 1998):

$$\Delta\theta_i = \dot{\theta}_i.T_s \quad (3)$$

In this equation, $\dot{\theta}_i$ denotes the instantaneous angular speed of encoder *i* and T_s the sampling period of the microcontroller. This relationship does not depend on the number of pulses per revolution, but shows that the error increases with the angular speed, which is therefore kept low for good accuracy.

Description of the control laws

The two control laws have been chosen for their ease of implementation, for their unconditional stability and for their simplicity of adjustment. In order to verify all these properties that have been demonstrated on applications in vibration control of bending dynamics, we demonstrate here that they keep these properties in the case of an application in rotating machines. The parameters to be set are directly related to the passive damper and are very limited in number (one or two parameters). It is therefore not necessary to have a predictive model of the rotating machine and the device retains a fail-safe mode in case of loss of activation energy. Furthermore, the amplification gain is only dedicated to the adjustment of the vibration attenuation performance and does not impact the stability of the active system. In the case of the experimental application made on the present

academic bench, this gain was essentially limited by the physical performance of components such as the rotating collector or the current amplifier.

In a very direct and natural way, both control laws use a single variable feedback loop. This variable was chosen in a very direct way also as being the velocity fluctuations between the two ends of the shaft (torsional velocity) since it is the target manifestation to be attenuated. The α-HMD controller was chosen as it provides optimal performance in reducing the vibration level at the target frequency of the TMD. The skyhook controller is known for its performance in the sense of the H2 standard, which is why it was included in this study. From a purely theoretical point of view, there were no particular implementation problems and the two controllers were introduced without any notable theoretical or conceptual modification compared to their bending vibration version. This is a strong demonstration of their ease of use and their robustness regarding the application domain, particularly for rotating machines, since the TMD has been tuned with very classical methods also usely provided for bending vibration

The only limitations encountered are constraints and limits imposed by the technological solutions chosen for the academic demonstrator. In particular, we can mention the limitations due to the friction of the Voice Coils in their tangential translation (effect of centrifugal forces), the limitations due to the electrical circuit and the slip ring.

α-HMD

The logic of the so-called α-HMD is the addition of two new zeros in the closed-loop system, in the vicinity of the original pole of the mode to control. This addition is compensated for at high frequencies with the introduction of a pair of poles. The controller equation is therefore defined as:

$$H_\alpha(s) = g_\alpha \frac{(s+\alpha)^2}{s^2} \tag{4}$$

With g_α a gain value. (Collette and Chesné, 2016) shows that this filter is hyperstable as long as the parameter α (that gives the control strategy its name) remains between the frequencies of the two poles created by the adjunction of the TMD. Its optimal performance is reached when α is exactly equal to the original pole frequency. It acts indeed as a phase rectifier for the open loop transfer function, to compensate for the drops caused by the two resonances.

This controller is then added in a velocity feedback loop, with a resulting torque C_a given as:

$$C_a(s) = H_\alpha(s).\Delta\dot{\theta} \tag{5}$$

In this expression, $\Delta\dot{\theta}$ is the difference of angular speeds between the two sides of the torsion shaft. In practice, a high-pass filter with very low cut-off frequency is also added in the loop, in order to remove the constant component of the measure of $\Delta\dot{\theta}$. The result of this control law in the feedback loop is an amplification of the stroke of the actuator, which therefore amplifies the effect of the passive TMD on the primary structure.

Skyhook emulation

On the contrary, the Skyhook control strategy (also called HSHMD) is designed as the adjunction of an additional "damping", in parallel to the passive behavior of the TMD. In this configuration, the dashpot is linked to a virtual "ground", which enables a withdrawal of energy from the primary structures, and eventually a vibration mitigation. The situation is depicted in Figure 4, where I_{VC} stands for the inertia provided by the Voice Coils, I_{eq} is the equivalent inertia involved in the vibration of the structure, and ψ_1 and ψ_{vc} are the angular coordinates relative to θ_2 (the difference of the absolute degree of freedom and θ_2).

The emulation of such a damper is accomplished by matching the desired damper behavior to the equation of motion of the actuator. The process is fully described in (Chesné, 2022), and gives the following filter equation:

$$H_{SH}(s) = c_{SH}.\left(1 - \frac{\psi_{VC}}{\psi_1}\right)^{-1} = \frac{c_{SH}}{s^2}.\left(s^2 + \frac{c_{VC}}{I_{VC}}s + \left(\frac{2\pi f_c}{1+\mu}\right)^2\right) \quad (6)$$

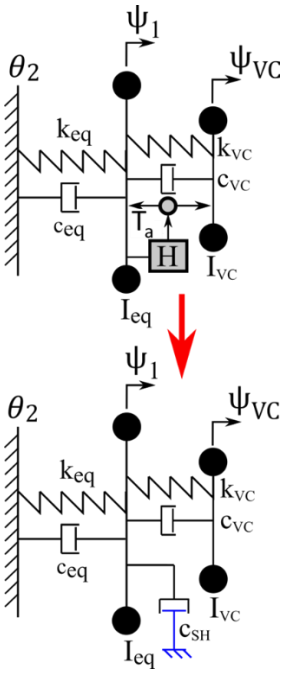

Figure 4. Mechanical analogy of the emulated Skyhook damper. The parameters ψ correspond to a change of variable, to consider the global rotation of the shaft.

The result is very close to the previous equation (4), when $(s+\alpha)^2$ is expended, and the parameter α set to its optimal value $2\pi f_c$. The second "damping" term is on the contrary quite different. In (6), c_{SH} is the gain of the controller when a Skyhook control strategy is applied. This equation is as before introduced in a velocity feedback loop, which gives for the actuator torque:

$$C_a(s) = H_{SH}(s).\Delta\dot{\theta} \quad (7)$$

Experiments for analyzing the effects of the control laws

The two control laws are tested on the test rig, using a dSPACE interface, operated with MATLAB Simulink. Various values for the gain of each law are tested to understand their impact.

The rotation target regime is set to 60 rpm (1 Hz) in order to assume a global speed of the shaft with good stationary conditions. In the present study, the servomotor has to assume the main speed of the shaft and to feed some excitations in torque at different frequencies. But the most perturbating effect of speed operates on the translation movement of VCAs with a damping modification due to the stick effect introduced by some centrifugal forces. These are the limitations in speed which have been deduced by the authors to their best understanding in order to compare efficiency and performance of active controls proposed.

The perturbation consists in a sine swipe from 0 to 75 Hz, with a magnitude of 1.11 N.m and a phase set at 0 rad (relatively to the encoder of the servomotor). It is assessed with a measurement of the current in the servomotor, which is proportional to the torque exerted on the shaft. The output signal is the torsion determined by the encoders. After filtering (High-pass filter to remove the constant component and notch filter to remove specific harmonics) and derivation, this data yields the input signal for the controller. In all tests, a current limitation is specified at 0.4 A in order to ensure a safe behavior of the demonstrator.

Semi-passive version

The first classical step in the hybridization of the damper is to close the electrical circuit, incorporating only the two VCAs (which therefore provide a resistance of 4.4 Ω and a self-inductance of 1.6 mH) and potentially an additional resistor R_c. Added resistance values of 22 Ω, 10 Ω and 5 Ω have been tested and results are depicted in Figure 5 with the gain of the FRF of the torsion after a frequency sweep of the torque fluctuation at an fixed operating speed of 120 rpm.

As it is well-known closing the circuit simulates the addition of a mass (circuit inductance) and additional damping (circuit resistance) to the TMD. As the stiffness is maintained in the absence of capacitance in the circuit, this necessarily leads to detuning of the TMD.

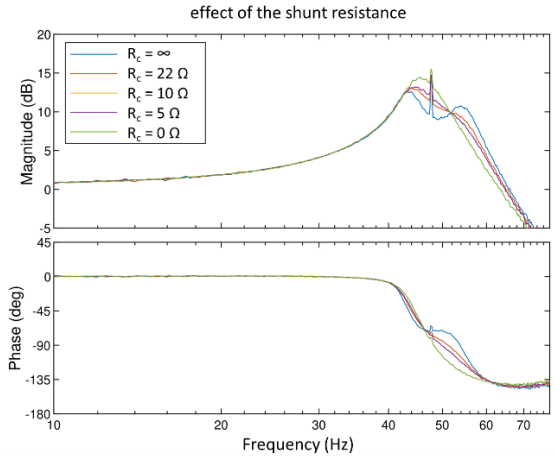

Figure 5. Effect of the shunt resistance in semi-passive configuration

In the non-shunted case ($R_c = \infty$), the expected passive behavior is well found, with the two "bumps" characteristic of the tuned system. This case is therefore representative of fail mode with a open electrical circuit. As the resistance under test decreases, the lowest frequency hump increases in amplitude and shifts in frequency to the right, while the highest frequency hump attenuates, to the point where it is no longer visible for a short-circuited (0 Ω) assembly. The whole system then tends towards a resonant system without a damper, in which the dampers are "stuck" to the primary system, thus adding their inertia to it.

Alpha-control strategy

Figure 6 compares three values of gain to the situation where no control is applied. The FRF of the torsion magnitude against the input torque clearly shows the effect of a gain increase, which is similar to an addition of inertia on the TMD. Indeed, the valley at the critical frequency is exacerbated, while the two characteristic peaks of a TMD sprawl over a broadened bandwidth. The vibration mitigation strategy performs well on a range of frequencies around the critical frequency, but does not prevent the overshoot caused by the pole spacing when the gain is increased. The maximum magnitude of vibration between 0 and 75 Hz is however reduced by 2.5 dB when a gain of 15000 N.ms/rad is used compared to the situation where no control is applied. At the critical frequency, this reduction reaches 12 dB.

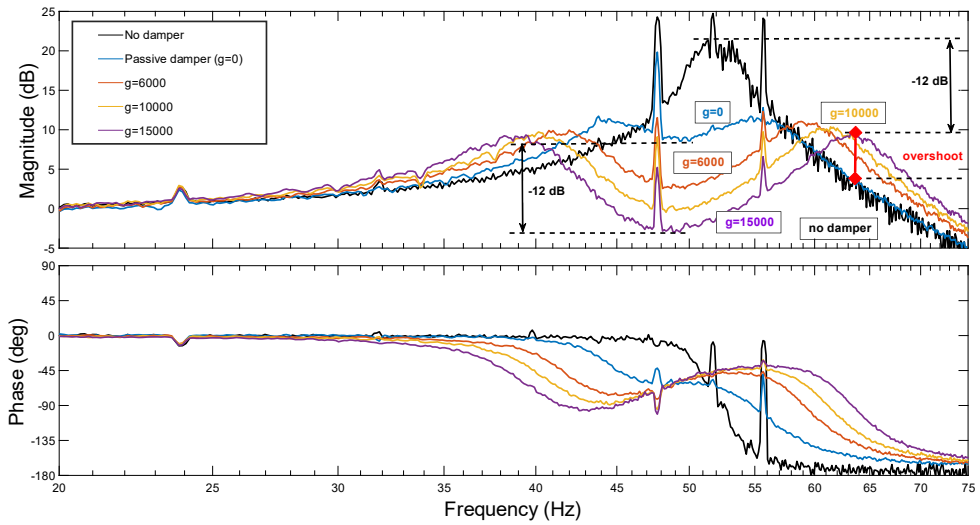

Figure 6. FRF torsion of the shaft against input torque, with α-control

One can also notice sharp peaks at 48 Hz and 56 Hz, and to a lesser extent at 24 Hz. These are parasitic excitation harmonics caused by the construction of the test rig itself (that was also used for the assessment of a hybrid damper, previously quoted, where magnets exert a cyclic torque). They are captured by the encoders but do not affect the servomotor, and consequently they can be ignored.

Skyhook damper strategy

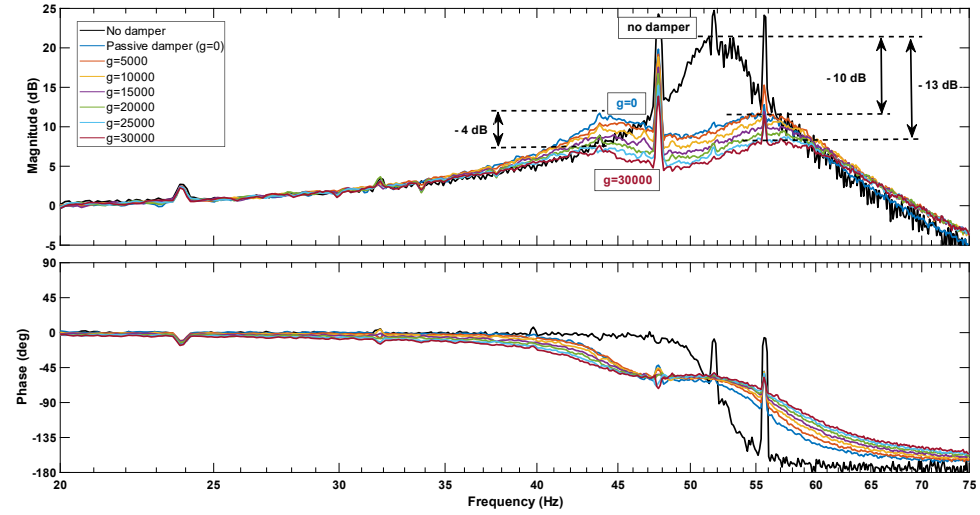

Figure 7. FRF torsion of the shaft against input torque, with Skyhook control

In Figure 7, the same test is run for the Skyhook control, except the gain has been increased every 5000 N.ms/rad up to 30000 N.ms/rad. Clearly, the magnitude of oscillation reduction is not as dramatic as before, but the reduction occurs on the whole bandwidth. No major re-amplification appears, except between 65 and 75 Hz, where it reaches 2 dB. However, this is not the case when $c_{SH} = 10000$, and for all the other runs, the amplification is exactly the same, which tends to indicate that this situation can be accounted for by a slight sensor or system change, and does not point out a responsibility of the control strategy. With a gain of 15000 N.ms/rad, the maximum magnitude of vibration is reduced by 2 dB (damping factor of 11% at the low frequency pole), and reaches 4 dB with 30000 N.ms/rad (damping

factor of 14%). With higher gains, the output current of the controller exceeds the limit of 0.4 A determined after the performances of the amplifier, and so no higher values have been investigated.

Root locus

In Figure 8, a plot of the root loci for the two control laws is displayed, to compare the experimental poles variation with the gain to the theoretical prediction. It shows that the experimental evolution is in good correlation with the prediction, especially for the Skyhook damper. The behavior with the α-control, where the lower branch reveals a growth of the real part, can be accounted for modifications of the critical frequency with the rotation speed and the excitation magnitude caused by the bench construction, thus changing the choice for α. A hint particularly points towards that direction: in the identification of the experimental poles and zeros, the frequency for the zero decreases slightly with the gain, which is not the case for the Skyhook emulation. The filters used during the measurement can also impact the result. However, the values measured remain close to the prediction, and confirm the difference of strategy for the two control laws: with the α-control, the spread of the poles is clear, whereas for the Skyhook the frequency is almost constant, and only the damping coefficient is affected.

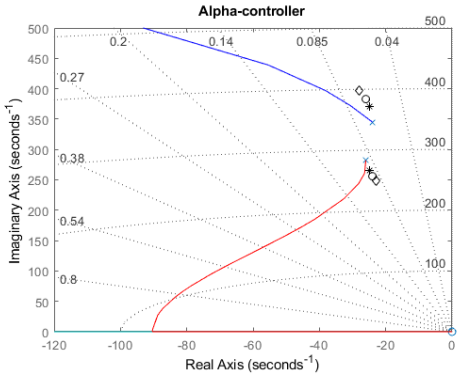

a. ∗ g=6000, o g=10000, ◊ g=15000

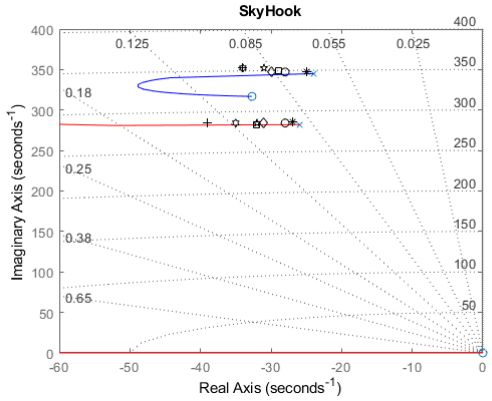

b. ∗ g= 5000, o g=6000, ◊ g=10000, □ g=15000, ☆ g=20000, ⬡ g=25000, + g=30000

Figure 8. Root loci for the α-control (a.) and Skyhook control (b.), with experimental results

Comparison and discussion

In this section, the results for the alpha-controller with a gain of 15000 N.ms/rad (max value for a current below 0.4A) is compared to the Skyhook with $c_{SH} = 15000$ (equal gain). Figure 9 shows the FRF between the output current of the generator and the torque exerted by the servomotor. One can notice that for low frequencies, the evolution is very similar for both control laws when the gain is the same.

Above 20 Hz, the gap increases both in phase and in magnitude. At 52 Hz, the critical frequency, the phase gap is 30° whereas the output current is 2 dB higher for the α-controller than for the Skyhook, for the same excitation. For higher frequencies, the gap between the control laws keeps on increasing, whereas no major impact on vibration reduction can be spotted. This suggests that the α-controller delivers more current at the highest frequencies than the Skyhook controller, but out of phase with the oscillation to reduce.

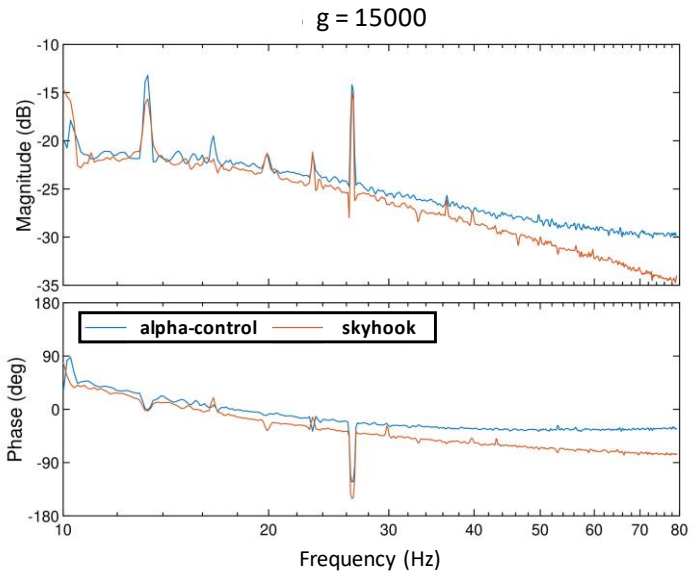

Figure 9. FRF output control current against input torque

This chart is completed with Figure 10, where the measured output current resulting from a sine swipe excitation and its RMS value are displayed, after a low-pass filter (cutoff frequency at 400 Hz for a sampling frequency of 1200 Hz). The trends are different due to the influence of the others harmonics, but confirms that the energy delivered by the alpha-controller is greater than that for the Skyhook for the same gain. This also means that the perturbations of the bench are more affected around the critical frequency for the α-controller (apparition of two peaks on the blue curve) and at the highest frequencies for the Skyhook (proximity of the blue and black curves).

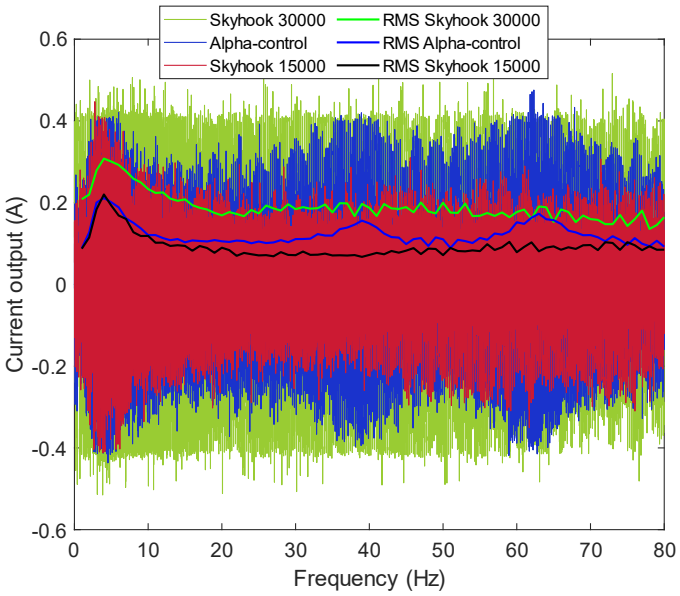

Figure 10. Filtered control current signal and corresponding RMS values

A comparison of the Bode representation of the equations for the two filters (with a unitary gain) can also be found in Figure 11, and helps understanding the difference despite the proximity of the control laws: the alpha-control aims at a reduction close to the critical frequency whereas the Skyhook reduces the oscillation over the whole bandwidth. In both cases, the mitigation is allowed by a phase correction from the controller. This difference resides mostly in the coefficient of the second (imaginary) term for the zero in the control law, which is much smaller in the case of the Skyhook control strategy ($\frac{c_{VC}}{I_{VC}}$ vs 2α). To that extent, the valley in the magnitude plot is much more stressed in this strategy (-20dB), whereas the phase transition is much steeper. This explains why the overshoot of the two characteristic peaks is avoided in this strategy (the phase of the current control remains more or less in opposition), and also why the α-control performs better close to the resonance frequency (this difference of 20dB creates a much larger amplification factor). To that extent, the choice of the control strategy depends on the spectral content of the perturbation signal.

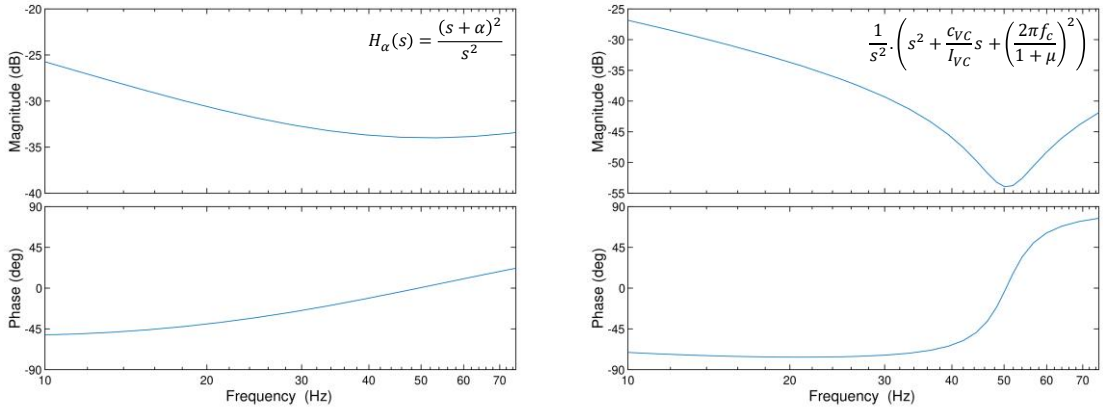

Figure 11. Bode diagrams of the two controllers with a unitary gain

Conclusion

In this paper, two recently-introduced control laws have been experimentally tested with success on a torsional system, opening new paths for vibration control strategies in rotational machines. By their direct implementation on an experimental setup, they have been demonstrated to be easy, robust and efficient in reducing torsional vibration with the same methodology in designing and setting governing parameters. Since the passive TMD is designed conforming classical methodology, these suggested control laws are based on a single variable feedback loop, this variable being the target for the vibration reduction. In summary, application of the methodology available for bending vibration has been revealed direct without theoretical or conceptual modifications with these hyperstable control laws. The only limitations encountered are constraints and limits imposed by the technological solutions chosen for the academic demonstrator.

The two laws perform well and have been compared in terms of performance and characteristics. With a limited control current of about 0.1 A_{RMS} (g = 15000), the maximum vibration magnitude over the whole investigated bandwidth is already 2 dB lower than a mere passive control with TMD. The investigation here is however limited to a rotation at 60 revolutions per minute. Future work on the topic will involve higher rotation speeds, in order to evaluate the robustness of the two laws to the change of damping coefficient in the Voice Coil under a radial charge caused by the inertial forces.

Based on this first experimental demonstration and validation, further investigations may be considered in the future about robustness of the control strategies for higher operating speeds, with mitigation of non-stationary operating speeds with larger bandwidth of excitation in frequency or more precise comparisons of the energy consumption of VCAs. To the best understanding of the authors, these

investigations require a dedicated design of the actuator as VCAs in translation acting in a tangential manner are subject to strong perturbating effects due to centrifugal forces.

Declaration of Conflicting interests

The authors declare that there are no potential conflicts of interest with respect to the research, authorship, and/or publication of this article.

Funding and acknowledgements

This work has been supported by the chair "Solutions for the future of Road Freight Transport", jointly created by INSA Lyon and Volvo Group.

References

Abouobaia E., Sedaghati R., Bhat R., 2020. Design Optimization and Experimental Characterization of a Rotary Magneto-Rheological Fluid Damper to Control Torsional Vibration. Smart Materials and Structures, vol. 29, no 4, p. 045010.

Aguirre G., Gorostiaga M., Porchez T., Munoa J., 2012. Self-Tuning Semi-Active Tuned-Mass Damper for Machine Tool Chatter Suppression, ISMA2012-USD2012, 2012, vol. 1, pp. 109-123.

Ahmadabadi Z. N., 2019. Nonlinear Energy Transfer from an Engine Crankshaft to an Essentially Nonlinear Attachment. Journal of Sound and Vibration, vol. 443, p. 139–154.

Alujević, N. Ćatipović, I. Malenica, Š. Senjanović, I. Vladimir N., 2020. Stability, performance and power flow of active U-tube anti-roll tank, Engineering Structures, vol. 211, p. 110267.

Auleley M., Thomas O., Giraud-Audine C., Mahé H., 2021. Enhancement of a Dynamic Vibration Absorber by Means of an Electromagnetic Shunt. Journal of Intelligent Material Systems and Structures, vol. 32, no3, pp. 331–354.

Cadiou, B., Stephan, C., Renoult, A., Michon, G., 2021. Damping adjustment of a nonlinear vibration absorber using an electro-magnetomechanical coupling, Journal of Sound and Vibration, vol. 518, p.116508. 10.1016/j.jsv.2021.116508.

Cao, B., Li, C., 2012. Design of active tuned mass damper based on robust control, in: 2012 IEEE International Conference on Computer Science and Automation Engineering (CSAE). Presented at the 2012 IEEE International Conference on Computer Science and Automation Engineering (CSAE), pp. 760–764, DOI 10.1109/CSAE.2012.6272877

Chesné, S., 2022. Hybrid Sky-Hook Mass Damper. Mechanics and Industry, 22 (3), DOI 10.1051/meca/2021050.

Chesné, S., Collette, C., 2018. Experimental validation of fail-safe hybrid mass damper. Journal of Vibration and Control 24, 4395–4406, DOI 10.1177/1077546317724949

Chesné, S., Inquieté, G., Cranga, P., Legrand, F., Petitjean, B., 2019. Innovative Hybrid Mass Damper for Dual-Loop Controller. Mechanical Systems and Signal Processing 115, 514–523, DOI 10.1016/j.ymssp.2018.06.023

Collette, C., Chesné, S., 2016. Robust hybrid mass damper. Journal of Sound and Vibration 375, 19–27, DOI 10.1016/j.jsv.2016.04.030

Dahaeze T., Collette C., 2021. Active Damping of Rotating Platforms Using Integral Force Feedback. Engineering Research Express, vol. 3, no 1, p. 015036.

Den Hartog, J., Ormondroyd, J., 1929. Torsional vibration dampers. Transactions of the American Society of Mechanical Engineering, no DOI.

Dong, X., Li, W., Yu, J., Pan, C., Xi, J., Zhou, Y., & Wang, X., 2020. Magneto-rheological variable stiffness and damping torsional vibration control of powertrain system, Frontiers in Materials, vol. 7, p. 121.

Gao P., Xiang C., Liu H., Walker P., Zhang N., 2019. Design of the Frequency Tuning Scheme for a Semi-Active Vibration Absorber. Mechanism and Machine Theory, vol. 140, pp. 641–653.

Haris A., Alevras P., Mohammapour M., Theodossiades S.,O' Mahony M., 202. Design and Validation of a Nonlinear Vibration Absorber to Attenuate Torsional Oscillations of Propulsion Systems. Nonlinear Dynamics, vol. 100, no 1, p. 33–49

Hosek M., Olgac N., Elmali H., 1999. The Centrifugal Delayed Resonator as a Tunable Torsional Vibration Absorber for Multi-Degree-of-Freedom Systems. Journal of Vibration and Control, vol. 5, no 2, p. 299–322.

Lai Y.-H., Chung L.-L., Chuang-Sheng W. Y., Wu L.-Y., 2018. Semi-active Phase Control of Tuned Mass Dampers for Translational and Torsional Vibration Mitigation of Structures. Structural Control and Health Monitoring, vol. 25, no 9, page e2191.

Meinhardt, C., Nikitas N., Demetriou, D., 2017. Application of a 245 metric ton Dual-Use Active TMD System, Procedia Engineering, vol. 199, pp. 1719-1724.

Nguyen, D.-C., 2020. Vibration control of a rotating shaft by passive mass-spring-disc dynamic vibration absorber. Archive of Mechanical Engineering 67, DOI 10.24425/AME.2020.131693

Nguyen, D.-C., 2019. Determination of optimal parameters of the tuned mass damper to reduce the torsional vibration of the shaft by using the principle of minimum kinetic energy. Proceedings of the Institution of Mechanical Engineers, Part K: Journal of Multi-body Dynamics 233, 327–335, DOI 10.1177/1464419318804064

Ormondroyd, J., Den Hartog, J.P., 1928. Theory of the dynamic vibration absorber. ASME Journal of Applied Mechanics, 50(7), pp.9-22, no DOI

Paillot, G., Chesné, S., Rémond, D., 2021. Hybrid coupled damper for the mitigation of torsional vibrations and rotational irregularities in an automotive crankshaft: Concept and design subtleties. Mechanics Based Design of Structures and Machines, DOI 10.1080/15397734.2021.1921595

Paillot G., Besnier E., Chesné S., Rémond D., 2023. Experimental validation of a new hybrid self-supplied crankshaft torsional vibrations damper, Mechanical Systems and Signal Processing, vol. 182, p. 109560, https://doi.org/10.1016/j.ymssp.2022.109560.

Paknejad, A., Zhao, G., Chesné, S., Deraemaeker, A., and Collette, C. Hybrid Electromagnetic Shunt Damper for Vibration Control. ASME. J. Vib. Acoust. April 2021; 143(2): 021010. https://doi.org/10.1115/1.4048389, (2020)

Preumont, A., Seto, K., 2008. Active control of structures. John Wiley & Sons, West Sussex, United Kingdom, ISBN: 978-0-470-03393-7

Preumont, A., Alaluf, D., Bastaits, R., 2014. Hybrid Mass Damper: A Tutorial Example. In: Hagedorn, P., Spelsberg-Korspeter, G. (eds) Active and Passive Vibration Control of Structures. CISM International Centre for Mechanical Sciences, vol 558. Springer, Vienna.

Qiu D., Seguy S., Paredes M., 2018. Tuned Nonlinear Energy Sink With Conical Spring : Design Theory and Sensitivity Analysis. Journal of Mechanical Design, vol. 140, no 1, p. 011404.

Remond, D., 1998. Practical performances of high-speed measurement of gear transmission error or torsional vibrations with optical encoders. Meas. Sci. Technol. 9, 347–353, DOI 10.1088/0957-0233/9/3/006

Rodriguez, J., Cranga, P., Chesne, S. , Gaudiller, L., 2018. Hybrid active suspension system of a helicopter main gearbox, J.Vibr. Control vol. 24, pp. 956–974.

Tso, M.H., Yuan, J., Wong, W.O., 2013. Design and experimental study of a hybrid vibration absorber for global vibration control. Engineering Structures 56, 1058–1069, DOI 10.1016/j.engstruct.2013.06.017

Umutlu, R., Ozturk, H., Bidikli, B., 2020. A robust adaptive control design for active tuned mass damper systems of multistory buildings. Journal of Vibration and Control, 27 (23-24),1–13, DOI 10.1177/1077546320966236

Vu, X.-T., Nguyen, D.-C., Khong, D.-D., Tong, V.-C., 2017. Closed-form solutions to the optimization of dynamic vibration absorber attached to multi-degrees-of-freedom damped linear systems under torsional excitation using the fixed-point theory. Proceedings of the IMechE 146441931772521, DOI 10.1177/1464419317725216

Wang J., Liu Y., Qin Z., Ma L., Chu F., 2022. Dynamic performance of a novel integral magnetorheological damper-rotor system, Mechanical Systems and Signal Processing, vol. 172, p. 109004, https://doi.org/10.1016/j.ymssp.2022.109004.

Yan, X., Xu, Z.-D., Shi, Q.-X., 2020. Fuzzy neural network control algorithm for asymmetric building structure with active tuned mass damper. Journal of Vibration and Control, 26 (21-22), DOI 10.1177/1077546320910003.